Available online at www.sciencedirect.com
SCIENCE DIRECT
Journal of Magnetic Resonance 179 (2006) 20–28
JMR Journal of Magnetic Resonance
www.elsevier.com/locate/jmr

Characterization of dynamic processes using deuterium in uniformly ^{2}H,^{13}C,^{15}N enriched peptides by MAS solid-state NMR

Maggy Hologne [a,1], Zhongjing Chen [a,2], Bernd Reif [a,b,*]

[a] Forschungsinstitut für Molekulare Pharmakologie (FMP) Robert-Rössle-Str. 10 13125 Berlin, Germany
[b] Charité Universitätsmedizin, D-10098 Berlin, Germany

Received 3 August 2005; revised 29 September 2005
Available online 11 November 2005

Abstract

We present in this paper ^{2}H,^{13}C MAS correlation experiments that are performed on a uniformly ^{2}H,^{13}C,^{15}N labeled sample of Nac-Val, and on the uniformly ^{2}H,^{15}N labeled dipeptide Nac-Val-Leu-OH. The experiments involve the measurement of ^{2}H T_1 relaxation times at two different magnetic fields, as well as the measurement of the ^{2}H tensor parameters by evolution of the ^{2}H chemical shift. The data are interpreted quantitatively to differentiate between different side chain motional models.

Keywords: MAS solid-state NMR; ^{2}H; Deuteration; Dynamics

1. Introduction

MAS solid-state NMR spectroscopy developed rapidly over the past years. Assignments of uniformly ^{13}C and ^{15}N enriched crystalline peptides and proteins, as well as the determination of their three-dimensional structure becomes now feasible [1–4]. Assignment techniques were successfully applied to a number of amyloidogenic peptides and proteins [5–8], and to membrane protein ligands [9,10]. Understanding the dynamics of a protein is, however, important for the characterization of its function.

The deuterium quadrupolar interaction, which dominates the spectral shape, is very sensitive to molecular motion over an extremely large kinetic window [11,12]. Three categories of motion can be distinguished [13]. Slow motion: the frequency of motion is greater than the quadrupolar coupling interaction ($10^{2} > \tau_C > 10^{-4}$ s). In general, no remarkable effects are observed on the ^{2}H 1D spectra. The effect can be quantified by selective inversion experiments, measurement of the decay of quadrupolar order or by 2D exchange spectroscopy [12,14–16]. Intermediate motions ($10^{-4} > \tau_C > 10^{-7}$ s) take place on the timescale of the quadrupolar coupling constant and have, therefore, an influence on the deuterium line shape. Intermediate time scale motions are usually studied by interpretation of line shape distortions in 1D spectra which are due to anisotropic T_2 relaxation [17–21]. In the fast motion limit ($10^{-7} > \tau_C > 10^{-12}$ s), the deuterium quadrupolar tensor is reduced compared to the static case. The anisotropy of the spin–lattice relaxation time T_1 allows a quantification of the timescale of the motional process and to assign a motional model [11,21–24].

In the past, deuterium labeling was used successfully to investigate molecular order and dynamics in solid-state NMR in a wide variety of crystalline and disordered systems, embracing surfaces, inclusion compounds, liquid crystals, polymers, membranes, or biological compounds [11,25]. Magic angle spinning was first applied by Pines and co-workers [26] to obtain information on dynamics. MAS ^{2}H NMR allows an increase in both sensitivity and

* Corresponding author. Fax: +49 30 94793 199.
E-mail address: reif@fmp-berlin.de (B. Reif).
[1] Present address: Laboratoire de RMN biomoléculaire, Université Claude Bernard Lyon 1, CNRS UMR 5180, 69622 Villeurbanne, France.
[2] Present address: Department of Chemistry, Room 5365, 1101 University Avenue, Madison WI 53706, USA.

1090-7807/$ - see front matter © 2005 Elsevier Inc. All rights reserved.
doi:10.1016/j.jmr.2005.10.014

signal to noise ratio to study dynamic processes [27–29]. First solid-state NMR experiments to study membrane dynamics were performed by Seelig [30] and Davis [31]. Introducing bilayer micelles (bicelles) resulted in a big step forward in the study of these systems [32]. Brown and co-workers [33] described a novel method which correlates ^{2}H NMR relaxation rates and order parameter calculations to understand the forces associated with bilayer deformation. With respect to membrane proteins, deuterium experiments describing dynamical properties of gramicidin A and S incorporated into liposomes were carried out by Dameta et al. [34]. Cross and co-workers[35] extended this approach and, e.g., determined the dynamics and structural properties for each of the valine side chains of oriented and amorphous gramicidin solubilized in hydrated lipid bilayers. Similarly, dynamic leucine and valine packing effects in phospholamban and glycophorin A were characterized by Smith and co-workers [36,37]. In aligned samples, deuterium labeling allowed the determination of the orientation of the retinal in bacteriorhodopsin under MAS conditions (MAOSS) [38]. In a static aligned sample, informations on the orientation and dynamics were obtained for ligands bound to the acetylcholine receptor [39]. In all these studies, deuterium had to be incorporated into the sample as a selective label.

Information on dynamics on uniformly carbon labeled samples was reported recently for aromatic ring flips in tyrosine-ethylester [40]. These effects were confirmed by HCCH and LG-CP type experiments [41]. Variations of the ^{15}N T_1 relaxation times were attributed to molecular dynamics in the backbone of the protein Crh [42]. In deuterated peptide samples, ^{2}H,^{13}C correlations were reported first by Sandström et al. [43] who substituted exchangeable protons by deuterium. Studies using perdeuterated proteins were performed by Hologne et al. [44] who obtained information about side chain dynamics in a uniformly ^{2}H,^{13}C,^{15}N isotopically enriched protein.

We introduced uniform deuterium isotopic labeling of peptides and proteins originally to reduce ^{1}H,^{1}H dipolar interactions. These experiments were pioneered in the solid-state by Griffin and co-workers[45,46] who could show that the ^{1}H line width is drastically reduced if the content of exchangeable ^{1}H is reduced with respect to ^{2}H in perdeuterated model compounds. Deuteration and back-substitution of exchangeable protons in peptides and proteins allows sensitive ^{1}H detection [47–49], determination of long range ^{1}H,^{1}H distances [50,51] and the localization of mobile water molecules in the protein structure [52]. This labeling schemes was inspired by solution state NMR investigations for large proteins (MW > 30 kDa) which use deuteration to decrease R_2 relaxation rates of H^N protons, and this way, to increase the effective resolution obtainable in these systems [53–57].

We present in this paper ^{2}H,^{13}C MAS correlation experiments that were performed on a uniformly ^{2}H,^{13}C,^{15}N labeled sample of Nac-Val, and on the uniformly ^{2}H,^{15}N labeled dipeptide (Nac-Val-Leu-OH). The experiments involve the measurement of the ^{2}H tensor parameters by evolution of the ^{2}H chemical shift, as well as the measurement of ^{2}H T_1 relaxation times at two different magnetic fields. Deuterium is exploited as well as by solution-state NMR spectroscopy as an active nucleus to obtain dynamic information [58,59]. In contrast to ^{15}N relaxation measurements, ^{2}H relaxation measurements can provide direct information on side chain dynamics which actually involve the chemical groups of interest which are important for protein function.

2. Experimental

Solid-state NMR experiments were performed at magnetic field strengths of 9.4 and 14.1 T, employing a Bruker Avance 400WB and Avance 600WB, respectively. In both cases, the spectrometer was equipped with a 4 mm triple resonance MAS probe. All experiments were acquired setting the MAS frequency to 10.0 kHz.

The presented data are based on 2D ^{2}H,^{13}C correlation experiments and can easily be extended to 3D ^{2}H,^{13}C,^{13}C experiments, if chemical shift dispersion in the carbon spin system is critical. The pulse sequences are sketched in Fig. 1. We take advantage of relatively short spin–lattice relaxation time T_1 of deuterium ($T_1 \sim 50$ ms for C–^{2}H$_3$). Therefore, the experiment is implemented starting with an excitation pulse on deuterium. The typical deuterium 90° pulse lengths was on the order of 3.5 μs on both spectrometers. After ^{2}H chemical shift evolution, magnetiza-

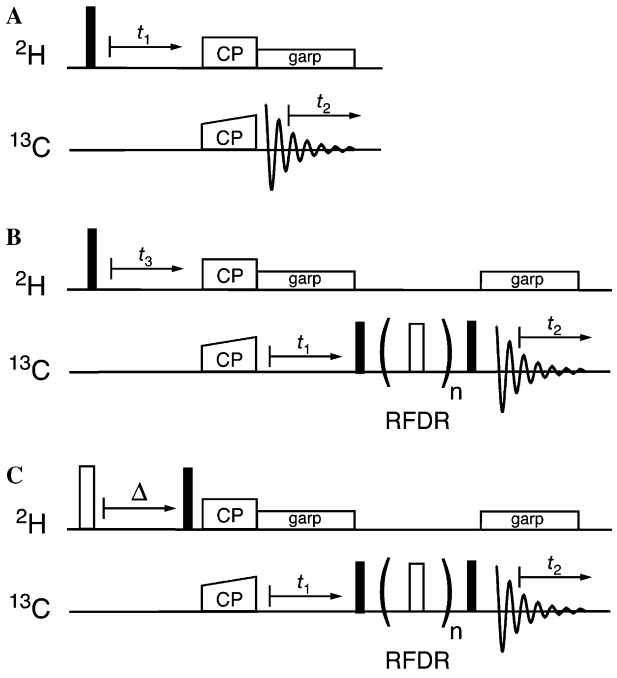

Fig. 1. ^{2}H,^{13}C CP MAS pulse sequences. (A) 2D ^{2}H,^{13}C CP MAS correlation. (B) 3D ^{2}H,^{13}C,^{13}C correlation. (C) ^{2}H T_1 recovery. RFDR mixing and an indirect ^{13}C evolution period t_1 can be implemented in (B and C), if the dispersion in the ^{13}C dimension is not sufficient to resolve an individual ^{13}C resonance.

tion is transferred from ^{2}H to ^{13}C using cross-polarization (CP) employing a CP mixing time of $\tau_{CP} = 2.5$ ms. The ^{2}H rf field for cross polarization was on the order of 40 kHz on both spectrometers. We find that application of decoupling of the ^{2}H–^{13}C scalar coupling using GARP [60] yields an improvement of the line width in the direct and indirect evolution period. The enhancement in resolution is on the order of the size of the $^{1}J_{^{2}H,^{13}C}$ scalar coupling (~20 Hz). The full width of a deuterium powder pattern can be on the order of 250 kHz, and an analog filter (~1 μs dwell-time) is needed to cover the complete spectral width. In 2D experiments, we used an increment of $t_1 = 1$ μs in the indirect ^{2}H dimension (spectral width = 500 kHz, 4k increments).

To obtain T_1 recovery curves (Fig. 1C), a ^{2}H π-pulse was implemented followed by a delay Δ which was varied from 1 ms to 1.5 s prior to the ^{2}H π/2 read-out pulse. Typically, we employ recycle delays on the order of 250 ms for 2D ^{2}H,^{13}C correlation experiments and on the order of 3 s for T_1 experiments. In case of spectral overlap, a RFDR ^{13}C,^{13}C mixing together with a second indirect chemical shift evolution period t_1 on ^{13}C can be optionally implemented. Typical ^{13}C,^{13}C mixing times are on the order of 50 ms. The described experiments are in particular conservative with respect to sample heating, since no proton decoupling is required in neither the ^{2}H, nor the ^{13}C evolution period.

3. Results

Fig. 2 displays ^{13}C 1D spectra in which ^{1}H,^{13}C (Fig. 2A) and ^{2}H–^{13}C (Fig. 2B) cross-polarization was used in order to transfer magnetization to carbons. A better signal-to-noise (S/N) ratio is achieved in case of the ^{1}H,^{13}C CP experiment using a fixed number of scans (S/N = 197, in comparison to S/N = 109 in case of ^{2}H,^{13}C CP). However, due to the short ^{2}H-T_1 relaxation time, ^{2}H,^{13}C CP yields in total similar sensitivity. Best results were obtained for $\tau_{CP[^{2}H,^{13}C]} = 2$ ms. In case of the ^{1}H,^{13}C CP experiment, protons were decoupled using TPPM ($\omega_{rf}/2\pi \sim 80$ kHz). Only direct transfers between directly bonded ^{13}C and ^{2}H are observed in case of the ^{2}H,^{13}C CP experiment. No magnetization transfer is observed to the carbonyl resonance in this experiment. This is an important prerequisite for the two- and three-dimensional correlation experiments presented below, since carbon chemical shift evolution is required to disperse the dynamic information obtained in the deuterium dimension.

1D ^{13}C spectra with and without ^{2}H decoupling are presented in Fig. 3. Application of GARP to decouple the scalar coupling between directly bonded ^{2}H and ^{13}C allows to resolve the ^{13}C,^{13}C coupling ($J \sim 35$ Hz) for methyl carbons in NAc-Val. ^{1}H dipolar decoupling during acquisition results only in a small improvement of the carbon C^{α} line width (no effect is observed for other carbon resonances in NAc-Val). ^{1}H decoupling is therefore omitted for the other experiments presented in this manuscript.

A typical ^{2}H rf field which can be experimentally implemented on our spectrometer is on the order of 70 kHz. To validate if the applied power is sufficiently strong to excite the full ^{2}H quadrupolar tensor (160 kHz), we carried out simulations using SIMPSON [61] (data not shown). In the simulation, a MAS rotation frequency of 10 kHz, a quadrupolar coupling constant $C_Q = 160$ kHz and an asymmetry parameter $\eta = 0$ is assumed. The ^{2}H rf field of the excitation pulse was then varied between 10 and 100 kHz. The calculations yields the same ^{2}H spectrum independent of the rf field of the excitation pulse, indicating that MAS samples all crystallite orientations. These simulations are in agreement with a study carried out by

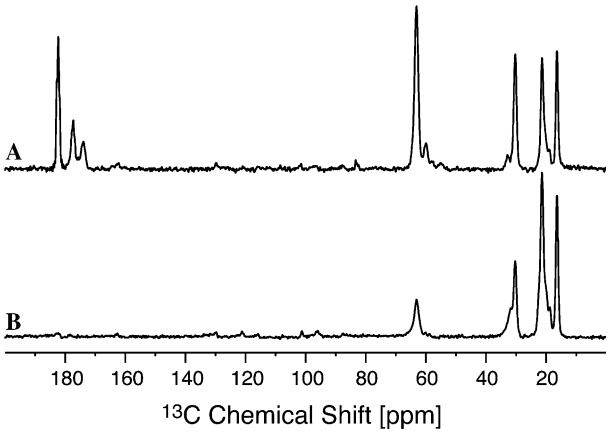

Fig. 2. ^{13}C 1D-spectra of u-[^{2}H,^{13}C,^{15}N]Nac-Val. (A) ^{1}H,^{13}C cross polarization is used to transfer magnetization to ^{13}C ($\tau_{CP} = 2$ ms, ^{1}H TPPM decoupling $\omega_{rf}/2\pi$ (^{1}H) = 80 kHz, NS = 4, S/N = 70/1). (B) ^{2}H,^{13}C cross polarization is employed to transfer magnetization to ^{13}C ($\tau_{CP} = 2.5$ ms, $\omega_{rf}/2\pi$ (^{2}H) = 40 kHz, NS = 32, S/N = 109/1). Typical $^{1}H^{N}$ T_1 and ^{2}H T_1 relaxation time are on the order of 3.0 s and 60 ms (for methyl groups), respectively (vide infra). The obtained signal-to-noise ratio per unit time is therefore comparable in both experiments.

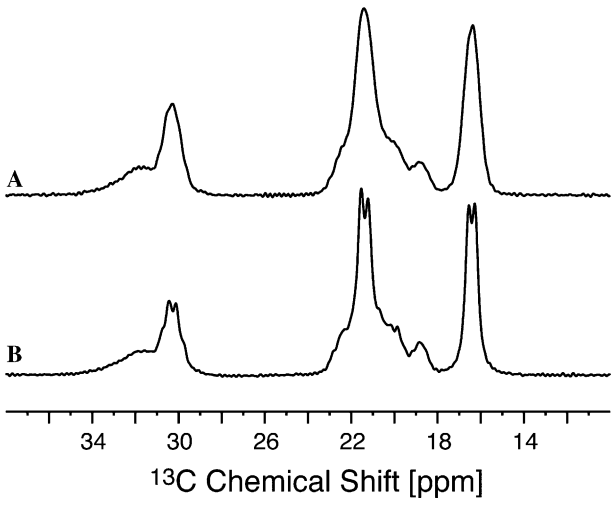

Fig. 3. ^{2}H–^{13}C CP 1D-spectra for u-[^{2}H,^{13}C,^{15}N]Nac-Val without (A) and with (B) decoupling of the scalar interaction to ^{2}H using GARP ($\omega_{rf}/2\pi \sim 2$–3 kHz).

Vega and co-workers [62] who describe the dynamics of magnetization transfer during cross-polarization between a spin-1 and a spin-1/2 nucleus using Floquet theory. For liquid crystalline samples, a theoretical description is provided by Emsley and co-workers [63,64].

3.1. Extraction of the ^2H quadrupolar coupling C_Q and the asymmetry parameter η

Fig. 4 represents experimental and simulated ^2H spectra for NAc-Val obtained in the indirect dimension, employing the pulse sequence represented in Fig. 1A. As expected, the quadrupolar tensor for the C^{α} bound deuterium covers the full width of 150 kHz, whereas the tensor for the methyl group deuterium atoms show a reduced anisotropy which is due to the fast methyl group rotation. ^2H spectra show no remarkable difference in ^2H isotropic chemical shift for C–^{2}H, C–$^2H_2$, and C–$^2H_3$ groups.

To fit the value for C_Q and η which are defined by the spinning side band intensities, a Fortran program is employed. As input, the program uses several fixed experimental interaction parameters (spinning frequency ω_r, spin number I, number of points, spectral width, number of spinning sidebands and intensities) which correspond to an initial set for the optimization process. The difference between calculated and experimental spinning sideband intensities are then minimized by modification [65] of the initial parameters using a non-linear least square regression based on Powell's method [66]. The uncertainties for each parameter are calculated from the variance–covariance matrix of the optimized parameter (using the sub-routine "sv02ac" in the Harwell library).

It is known that ^2H MAS spectra are sensitive to motion [29,67]. In order to determine the correlation time of the motion, ^2H NMR MAS spectra were simulated by calculating the time evolution of the complex magnetization through numerical integration of the stochastique Liouville equation [18,29,67,68] using the fourth-order Runge-Kutta method according to Merson (Harwell subroutine DA01A [69]). In the case of a rigid lattice, the envelope of the spectrum is a Pake doublet. The static electric field gradient tensor is axially symmetric along the C–^{2}H bond and the asymmetry parameter is zero. The anisotropy of the quadrupolar tensor is referred to as δ. In the presence of motion, however, the envelope of the spectrum changes and, assuming a specific motional model, the average electric field gradient tensor can be defined by an average anisotropy and asymmetry parameters, $\bar{\delta}$ and $\bar{\eta}$, respectively [20,70].

For C_α–^{2}H, the value determined for C_Q is typical for a static C–^{2}H bond. The shape of the spectrum reflects a Pake doublet and is characteristic for a rigid body. We can therefore exclude motional processes for this nucleus.

For methyl groups, the quadrupolar coupling constants fit to 50 kHz and the asymmetry parameter adopts a value of zero. Those results are typical results for methyl groups [11]. The small value of C_Q is due to fast rotational motion around the pseudo-threefold axis ($\bar{\delta}/\delta = 1/3$ and $\bar{\eta} = 0$).

The fit for C_β–^{2}H yields $C_Q = 104.4$ kHz and $\eta = 0.75$. Typical values for C–^{2}H moieties are $C_Q = 160$ kHz and $\eta = 0$. The observation of smaller values for C_Q and asymmetry parameters $\eta \neq 0$ indicates restricted motional processes. The value of the average quadrupolar coupling constant is related to the average anisotropy parameter.

For example, a typical chemical exchange between two conformations which are related by a jump angle of 120° (Markov process [71]) involves a narrowing of the envelope of the spectrum yielding an average asymmetry parameter $\bar{\eta} = 0.6$. $\bar{C}_Q$ is calculated by dividing C_Q by 5/8, which results in an effective quadrupolar coupling constant $\bar{C}_Q = 101.3$ kHz. We can directly exclude this jump model as a possible explanation for the observed effect, since a similar effect as observed for Val-β would be expected on the ^2H spectrum of Cγ–$^2H_3$. This is, however, not the case.

As a second explanation, the reduction in the apparent quadrupolar coupling constant for C_β–^{2}H can be accounted for by letting the bond wobble through a cone of half angle θ_0. If the orientational distribution within the cone is uniform, the quadrupolar coupling constant will be reduced by a factor

$$\cos\theta_c \frac{(1+\cos\theta_c)}{2}$$

A best fit for the cone half angle in our case is obtained if $\theta_c = 42°$.

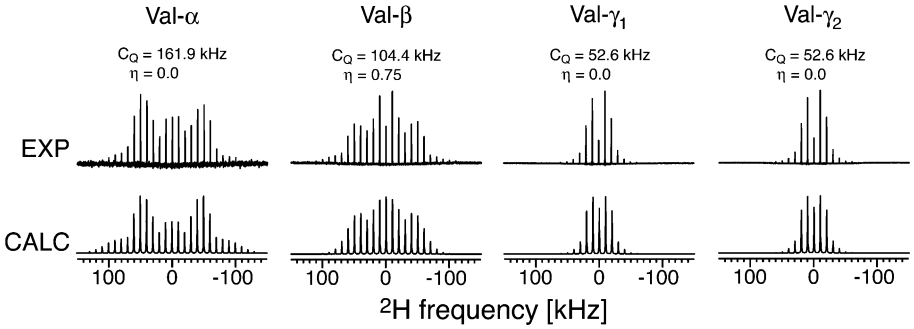

Fig. 4. Experimental and simulated ^2H MAS 1D-spectra for u-[^2H,^{13}C,^{15}N]Nac-Val. The represented 1D spectra correspond to the ^2H chemical shift for Val-α, $\delta(^{13}X) = 63.5$ ppm; Val-β, $\delta(^{13}X) = 30.8$ ppm; Val-γ_1, $\delta(^{13}X) = 16.5$ ppm and Val-γ_2, $\delta(^{13}X) = 22$ ppm. The fitted quadrupolar coupling constant and asymmetry parameter for each C–^{2}H group are indicated in the figure.

Third, if instead the bond motion is assumed to be confined to the surface of a cone, the reduction in splitting will equal

$$\frac{3\cos^2\theta_c - 1}{2},$$

which yields a cone half angle of 29° [72]. Thus, 29°–42° defines an approximate range of possible excursions of the bond C_β–^2H. To find out if the observed effect is indeed due to dynamics, a series of ^2H spectra as a function of temperature were recorded (see below).

Fig. 5 shows experimental and simulated ^2H spectra for the model dipeptide, u-[^2H,^{15}N]Nac-Val-Leu. ^{13}C was recorded at natural abundance. The two α-carbons in u-[^2H,^{15}N]Nac-Val-Leu fit to the same values of C_Q and η (C_Q = ca. 160.0 kHz, $\eta = 0.0$). The ^2H spectra for Val-β and Leu-γ can be fit assuming similar parameters for C_Q and η ($C_Q = 104.4$ kHz, $\eta = 0.65$ and $C_Q = 102.5$ kHz, $\eta = 0.61$, respectively). These tensor parameters are comparable to those found for Val-β in the sample u-[^2H,^{13}C,^{15}N]Nac-Val. Similar as in the case of Nac-Val, the tensor seems to be affected due to motion around the β-position of Val and the γ-position of Leu, respectively.

To better understand, if the tensor width observed for Val-β in Nac-Val, and Val-β and Leu-γ in Nac-Val-Leu is reduced due to dynamic processes, we recorded a series of 2D ^2H,^{13}C CP correlation experiments for Nac-Val within the temperature range +67 to −58 °C (Fig. 6), using the sequence represented in Fig. 1B. The deuterium signal in the indirect dimension consists of a train of rotational echoes. Fourier transformation of the entire echo train yields a spectrum which is split into spinning sidebands, the envelope of the spectrum reflects to first order the ^2H powder pattern line shape. The large deuterium anisotropy requires that the experiment is recorded using a very small increment (1 μs) in the indirect dimension. In order to obtain information on the actual ^2H T_2 relaxation time, we recorded a second 2D at each temperature using a multiple of the rotor period as an increment in the indirect dimension to observe the complete decay of the central transition. We find only small changes in line width as a function of temperature (Table 1). For example, the C–$^2H_3$ and C_β–^2H groups in

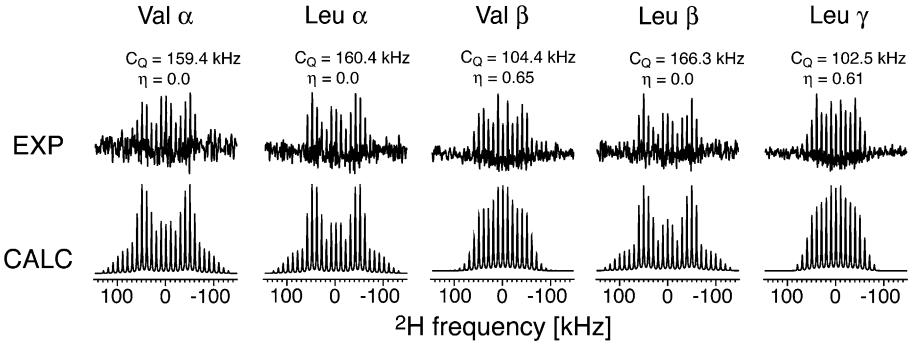

Fig. 5. Experimental and simulated ^2H MAS 1D-spectra for u-[^2H,^{15}N]Nac-Val-Leu recorded at ^{13}C natural abundance. 1D spectra correspond to the ^2H chemical shift of Val-α, $\delta(^{13}X) = 57$ ppm; Leu-α, $\delta(^{13}X) = 55.4$ ppm; Val-β, $\delta(^{13}X) = 30.1$ ppm; Leuβ, $\delta(^{13}X) = 35$ ppm; and Leu-γ, $\delta(^{13}X) = 28.75$ ppm. The fitted quadrupolar parameters for each C–^2H group are indicated in the figure.

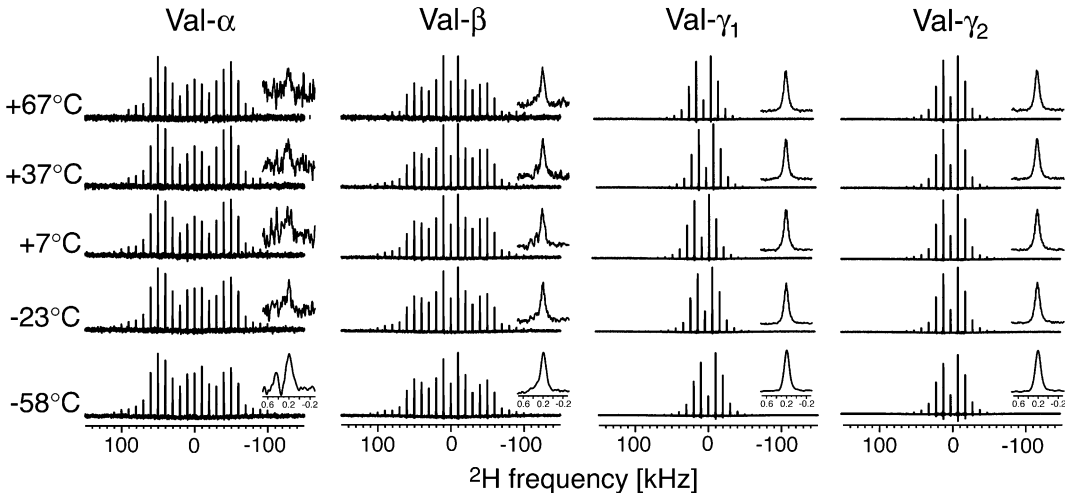

Fig. 6. Experimental MAS 1D ^2H spectra for Val-α, Val-β, Val-γ_1 and Val-γ_2 of u-[^2H,^{13}C,^{15}N]Nac-Val in the temperature range of 67 to −58 °C, using the pulse sequence displayed in Fig. 1A. The insets represent the ^2H isotropic chemical shift setting the t_1 increment to a multiple of the rotor period. The spectra were recorded at a magnetic field strength corresponding to a ^1H Larmor frequency of 400 MHz.

Table 1
^{2}H line width as function of temperature for Nac-Val as a function of the temperature (recorded at 400 MHz ^{1}H Larmor frequency)

Temperature (°C)	$\Delta\nu[^2H_3–C\delta_1]$ (Hz)	$\Delta\nu[^2H_3–C\delta_2]$ (Hz)	$\Delta\nu[^2H_2–C\beta]$ (Hz)	$\Delta\nu[^2H–C\alpha]$ (Hz)
+67	95	100	90	90
+37	95	100	100	100
+7	100	105	100	130
−23	115	120	100	150
−58	130	130	130	155

Nac-Val show a line width on the order of 90 Hz at +67 °C and on the order of 130 Hz at −58 °C. At the same time, the envelope of the spinning side band pattern for the respective chemical groups does not change upon variation of the temperature. Beshah and Griffin [73] studied ^{2}H line shape distortions for the methyl group of Nac-Val, and found no change in the spectral shape in the temperature range of 22 to −130 °C. We therefore conclude that lower temperatures would be required to properly address this question. At this point, however, temperatures below −100 °C are not accessible at our instrumental setup.

3.1.1. ^2H T_1 measurements

To have a complimentary measure for dynamics, we determined ^{2}H-T_1 relaxation rates for u-[^{2}H,^{15}N,^{13}C]-NAc-Val (Fig. 7). For this purpose, the pulse sequence represented in Fig. 1C was implemented. Since all ^{13}C chemical shifts are resolved in NAc-Val, an ^{13}C indirect dimension as well as ^{13}C,^{13}C mixing were omitted. The experimental results are represented in Fig. 7. As can be seen in Fig. 7, inversion is not quantitative. We found that the pulse length affects the inversion profile. However, higher ^{2}H rf fields than 70 kHz were not feasible on the employed probe. Therefore, we used experimentally a composite ^{2}H 180° pulse proposed by Levitt [74] $(\pi/4)_x - (\pi)_y - (\pi/2)_{-x} - (\pi)_y - (\pi/4)_x$ for the ^{2}H-T_1 experiments. The ^{2}H-T_1 relaxation times were obtained by fitting the experimental curves assuming an exponential dependence according to the formula

$$y = A_1 \cdot \exp\left(\frac{-x}{T_1}\right) + y_0.$$

All fitted values for ^{2}H-T_1 relaxation times are summarized in Table 2. As expected, we observe three different ^{2}H-T_1 recovery curves for C–^{2}H, C–^{2}H$_2$, and C–^{2}H$_3$. Methyl groups have short ^{2}H-T_1 relaxation times due to the rapid reorientation of the methyl group. The curves displaying Cβ-^{2}H and Cα-^{2}H are significantly different from one another. The longer T_1 time for Cα-^{2}H is in agreement with the assumption that the backbone in Nac-Val behaves like a rigid body. The intermediate ^{2}H-T_1 relaxation time observed for Cβ-^{2}H might indicate that the side chain undergoes a restricted motion, as we speculated above.

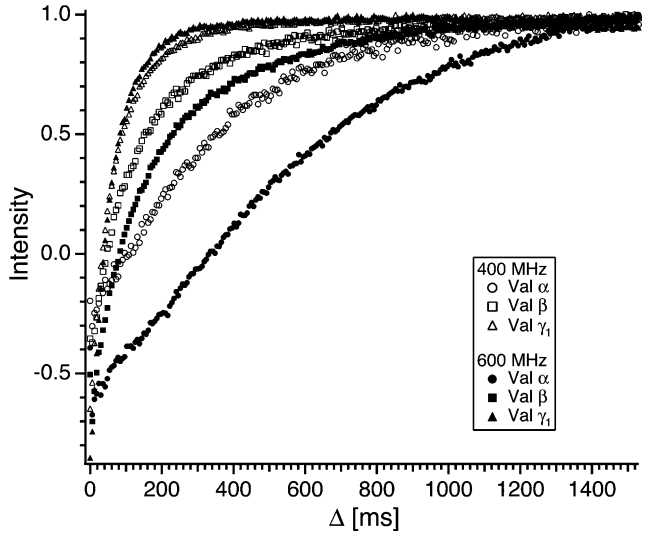

Fig. 7. $^2H_1$-T_1 recovery curves for Val-α, Val-β and Val-γ_1 of u-[^{2}H,^{13}C,^{15}N]Nac-Val at a magnetic field strength of 400 and 600 MHz.

Table 2
Fit values for ^{2}H-T_1 in NAc-Val

	400 MHz T_1 (ms)	600 MHz T_1 (ms)
C^2H_3 ($\delta = 16.5$ ppm)	72.6 ± 2.1	60.7 ± 1.2
C^2H_3 ($\delta = 21.5$ ppm)	66.6 ± 2.3	59.3 ± 1.5
$C_\beta{}^2H$ ($\delta = 30.5$ ppm)	145.9 ± 5.3	180.5 ± 10.0
$C_\alpha{}^2H$ ($\delta = 63.5$ ppm)	388.2 ± 16.9	844.2 ± 98.9

General expressions for relaxation rates for a variety of coupling mechanisms are derived by Spiess [75]. In the case of quadrupolar relaxation of deuterium, a general expression for T_1 is given by Torchia and Szabo [76]:

$$\frac{1}{T_1} = \frac{3\pi^2}{2}\left(\frac{e^2 q_{zz} Q}{h}\right)^2 (J_1(\omega_o) + 4 \times J_2(2\omega_0)). \quad (1)$$

$J_1(\omega_0)$ and $J_2(2\omega_0)$ are the spectral density functions corresponding to single quantum spin flips and to two-quantum spin flips, respectively. These spectral density functions are defined as

$$J_m(\omega_0) = 2\int_0^\infty C_m(t)\cos(\omega t)\mathrm{d}t, \quad (2)$$

where the autocorrelation function $C_m(t)$ is given by [76]:

$$C_m(t) = \sum_{a,a'=-2}^{2} d^2_{ma}(\theta_p) d^2_{ma'}(\theta_p) \exp\left[\mathrm{i}(a-a')\varphi_p\right] C_{aa'}(t). \quad (3)$$

d^2_{ma} are the usual reduced second-rank Wigner rotation matrix elements [77]. The $C_{aa'}(t)$ are the correlation functions describing the reorientation of the unique principal axis in the arbitrary molecular axis system. Torchia and Szabo [76] developed explicit expressions for the values of T_1 for different types of motions for solids based on the orientation dependence of the spin–lattice relaxation time.

For example, if a C–^{2}H bond vector is considered which can jump between two equivalent sites, the expression for T_1 is given by

$$\frac{1}{T_1}=\frac{\omega_Q^2}{2}\sin^2(2\Theta)\left\{\begin{array}{l}\frac{\tau}{1+\omega_I^2\tau^2}\left[\cos^2\theta+\cos^2(2\theta)-\cos(2\varphi)\left(\frac{3}{4}\sin^2(2\theta)-\sin^4\theta\right)\right]\\+\frac{\tau}{1+4\omega_I^2\tau^2}\left[4\sin^2\theta+\sin^2(2\theta)-4\sin^4\theta\cos(2\phi)\right]\end{array}\right\},\tag{4}$$

where $\tau=(k_{12}+k_{21})^{-1}$ and $\omega_Q=\frac{3e^2qQ}{4\hbar}$

The orientation of the magnetic field in the crystal-fixed coordinate system is described by the polar angles θ and ϕ. Θ represents the angle between the Z-axis of the principal axis and the crystal fixed coordinate system.

For a C–^{2}H bond that jumps between three equivalent sites (reorientation of a methyl group), T_1 can be expressed as

$$\frac{1}{T_1}=\frac{\omega_Q^2}{8}\left\{\begin{array}{l}\frac{\tau}{1+\omega_I^2\tau^2}\left[\begin{array}{l}\sin^2(2\Theta)(\cos^2\theta+\cos^2(2\theta))\\+\sin^4\Theta\left(\sin^2\theta+\frac{1}{4}\sin^2(2\theta)\right)\\-8\sin^3\Theta\cos\Theta\sin^3\theta\cos\theta\cos(3\phi)\end{array}\right]\\+\frac{\tau}{1+4\omega_I^2\tau^2}\left[\begin{array}{l}4\sin^2(2\Theta)\left(\sin^2\theta+\frac{1}{4}\sin^2(2\theta)\right)\\+\sin^4\Theta(1+6\cos^2\theta+\cos^4\theta)\\+8\sin^3\Theta\cos\Theta\sin^3\theta\cos\theta\cos(3\phi)\end{array}\right]\end{array}\right\},\tag{5}$$

where $\tau=(3k)^{-1}$For a methyl group ($\Theta=70.5°$) in the extreme narrowing limit, Eq. (5) becomes:

$$\frac{1}{T_1}=\frac{4\omega_Q^2\tau}{9}\left(1+\cos^2\theta\right)\tag{6}$$

Note that the expression for T_1 in this case is independent of the Larmor frequency ω_I, but dependent of the powder polar angle θ.

If the C–^{2}H bond diffuses freely around an axis, T_1 can be described as

$$\frac{1}{T_1}=\frac{\omega_Q^2}{8}\left\{\begin{array}{l}\frac{\tau_1}{1+\omega_I^2\tau_1^2}\times\sin^2(2\Theta)(\cos^2\theta+\cos^2(2\theta))\\+\frac{\tau_2}{1+\omega_I^2\tau_2^2}\times\sin^4\Theta\left(\sin^2\theta+\frac{1}{4}\sin^2(2\theta)\right)\\+\frac{\tau_1}{1+4\omega_I^2\tau_1^2}\times4\sin^2(2\Theta)\left(\sin^2\theta+\frac{1}{4}\sin^2(2\theta)\right)\\+\frac{\tau_2}{1+4\omega_I^2\tau_2^2}\times\sin^4\Theta(1+6\cos^2\theta+\cos^4\theta)\end{array}\right\},\tag{7}$$

where $\tau_1=(D)^{-1}$ and $\tau_2=(4D)^{-1}$. In the extreme narrowing limit for a methyl group, one obtains

$$\frac{1}{T_1}=\frac{8\omega_Q^2\tau_1}{27}.\tag{8}$$

Note that T_1 is independent of θ in case of free diffusion. In contrast to the three-site jump model, the entire powder pattern relaxes with the same relaxation time in this case.

Since different motional models have a different dependence on Θ, we expect that field dependent studies should allow the identification of a specific motional process. ^{2}H-T_1 recovery curves were therefore recorded for Nac-Val employing two different magnetic fields, 400 and 600 MHz. We observe shorter ^{2}H-T$_1$ relaxation times for Cβ–^{2}H and Cα–^{2}H at 400 MHz compared to 600 MHz, as expected from Eqs. (4) and (8) (jump or diffusion model, respectively). If no motion or very slow motional processes are assumed ($\tau_C > 5.10^{-2}$ s), the difference for ^{2}H-T_1 relaxation times recorded at an external magnetic field corresponding to 400 and 600 MHz is significant (around 115%). If a faster motional process is assumed ($\tau_C < 10^{-3}$ s), the difference decreases to few percent. For methyl groups, in the case of motion in the extreme narrowing limit, no field dependence is expected. The experimental values are indeed comparable at the two magnetic field strengths. Surprisingly, we observe a strong field dependence for the ^{2}H-T_1 relaxation time of Cα–^{2}H. Further studies have to be carried out to better understand the above described effects.

4. Conclusion

We could show in this manuscript, that deuterium spectroscopy on uniformly ^{2}H,^{13}C,^{15}N enriched peptides and proteins is feasible in MAS solid-state NMR. These experiments open up a wealth of dynamic information which was to this extend so far not accessible for solid-state NMR. The experiments are in particular conservative with respect to the applied power, since no ^{1}H high power decoupling is required during detection of the ^{13}C spins.

Acknowledgment

This research was supported by the DFG Grant Re1435.

References

[1] K. Nomura, K. Takegoshi, T. Terao, K. Uchida, M. Kainosho, Three-dimensional structure determination of a uniformly labeled molecule by frequency-selective dipolar recoupling under magic-angle spinning, J. Biomol. NMR 17 (2000) 111–123.
[2] C.M. Rienstra, L. Tucker-Kellogg, C.P. Jaroniec, M. Hohwy, B. Reif, M.T. McMahon, B. Tidor, T. Lozano-Pérez, R.G. Griffin, De novo determination of peptide structure with solid-state MAS NMR spectroscopy, Proc. Natl. Acad. Sci. USA 99 (2002) 10260–10265.
[3] F. Castellani, B.-J. van Rossum, A. Diehl, M. Schubert, K. Rehbein, H. Oschkinat, Structure of a protein determined by solid-state magic-angle spinning NMR, Nature 420 (2002) 98–102.
[4] S.G. Zech, A.J. Wand, A.E. McDermott, Protein structure determination by high-resolution solid-state NMR spectroscopy: application to microcrystalline ubiquitin, J. Am. Chem. Soc. 127 (2005) 8618–8626.
[5] A.T. Petkova, Y. Ishii, J.J. Balbach, O.N. Antzutkin, R.D. Leapman, F. Delaglio, R. Tycko, A structural model for Alzheimer's β-amyloid fibrils based on experimental constraints from solid state NMR, Proc. Natl. Acad. Sci. USA 99 (2002) 16742–16747.
[6] C.P. Jaroniec, C.E. MacPhee, N.S. Astrof, C.M. Dobson, R.G. Griffin, Molecular conformation of a peptide fragment of transthyretin in an amyloid fibril, Proc. Natl. Acad. Sci. USA 99 (2002) 16748–16753.
[7] A.B. Siemer, C. Ritter, M. Ernst, R. Riek, B.H. Meier, High-resolution solid-state NMR spectroscopy of the prion protein HET-s in its amyloid conformation, Angew. Chem. Int. Ed. 44 (2005) 2441–2444.
[8] C. Ritter, M.-L. Maddelein, A.B. Siemer, T. Lührs, M. Ernst, B.H. Meier, S.J. Saupe, R. Riek, Correlation of structural elements and infectivity of the HET-s prion, Nature 435 (2005) 844–848.
[9] S. Luca, J.F. White, A.K. Sohal, D.V. Filippov, J.H. van Boom, G.R. and, M. Baldus, The conformation of neurotensin bound to its G

protein-coupled receptor, Proc. Natl. Acad. Sci. USA 100 (2003) 10706–10711.
[10] L. Krabben, B.J. van Rossum, F. Castellani, E. Bocharov, A.A. Schulga, A.S. Arseniev, C. Weise, F. Hucho, H. Oschkinat, Towards structure determination of neurotoxin II bound to nicotinic acetylcholine receptor: a solid-state NMR approach, FEBS Lett. 564 (2004) 319–324.
[11] G.L. Hoatson, R.L. Vold, ^{2}H NMR spectroscopy of solids and liquid crystals, NMR Basic Principles Prog. 32 (1994) 3–61.
[12] K. Schmidt-Rohr, H.W. Spiess, Multidimensional Solid-State NMR and Polymers, Academic Press, London, 1994.
[13] E.B. Brouwer, G.D. Enright, J.A. Ripmeester, Solid-state NMR and diffraction studies of a Tunable p-tert-butylcalix (4)arene guest structure, J. Am. Chem. Soc. 119 (1997) 5404–5412.
[14] D. Reichert, Z. Olender, R. Poupko, H. Zimmermann, Z. Luz, Deuterium 2D exchange NMR by rotor synchronized nMAS, J. Chem. Phys. 98 (1993) 7699–7710.
[15] M.J. Brown, R.L. Vold, G.L. Hoatson, Selective inversion investigations of slow molecular motion in solid state deuteron NMR spectroscopy, Solid State Nucl. Magn. Reson. 6 (1996) 167–185.
[16] V. Gérardy-Montouillout, C. Malveau, P. Tekely, Z. Olender, Z. Luz, ODESSA a new 1D NMR exchange experiment for chemically equivalent nuclei in rotating solids, J. Magn. Reson. Ser. A 123 (1996) 7–15.
[17] M.M. Maricq, J.S. Waugh, NMR in rotating solids, J. Chem. Phys. 70 (1979) 3300–3316.
[18] D. Suwelack, W.P. Rothwell, J.S. Waugh, Slow molecular motion detected in the NMR spectra of rotating solids, J. Chem. Phys. 73 (1980) 2559–2569.
[19] R.J. Wittebort, E.T. Olejniczak, R.G. Griffin, Analysis of deuterium nuclear magnetic resonance line shapes in anisotropic media, J. Chem. Phys. 86 (1987) 5411–5420.
[20] H. Spiess, Deuteron NMR—a new tool for studying chain mobility and orientation in polymers, Adv. Polym. Sci. 66 (1985) 23–58.
[21] J. Hirschinger, H. Miura, K.H. Gardner, A.D. English, Segmental dynamics in the crystalline phase of Nylon66: solid state 2H NMR, Macromolecules 23 (1990) 2153–2169.
[22] R.L. Vold, G.L. Hoatson, T.Y. Tse, Effects of slow motion on deuteron relaxation time anisotropy, Chem. Phys. Lett. 263 (1996) 271–275.
[23] A. Scheicher, K. Müller, G. Kothe, Two dimensional NMR relaxation spectroscopy of molecular solids, J. Chem. Phys. 92 (1990) 6432–6440.
[24] F. Benevelli, A. Bond, M. Duer, J. Klinowski, Chloroform encapsulated in p-tert-butylcalix[4]arene: structure and dynamics, Phys. Chem. Chem. Phys. 2 (2000) 3977–3981.
[25] M.J. Duer, Solid-state NMR studies of molecular motion, Annual Reports on NMR Spectroscopy 43 (2001) 1–58.
[26] J. Ackerman, R. Eckman, A. Pines, Experimental results on deuterium NMR in the solid state by magic angle sample spinning, Chem. Phys. 42 (1979) 423–428.
[27] R.J. Schadt, E.J. Cain, A.D. English, Simulation of one-dimensional ^{2}H NMR line shapes, J. Phys. Chem. 97 (1993) 8387–8392.
[28] O. Weintraub, S. Vega, Dynamic ^{2}H nuclear magnetic resonance of rotating solids, Solid State Nucl. Magn. Reson. 4 (1995) 341–351.
[29] M. Hologne, J. Hirschinger, Molecular dynamics as studied by static-powder and MAS 2H NMR, Solid State NMR 26 (2004) 1–10.
[30] J. Seelig, Deuterium magnetic resonance: theory and application to lipid membranes, Q. Rev. Biophys. 10 (1977) 353–418.
[31] J. Davis, The description of membrane lipid conformation, order and dynamics by 2H NMR, Biochim. Biophys. Acta 737 (1983) 117–171.
[32] N.E. Gabriel, M.F. Roberts, Spontaneous formation of stable unilamellar vesicles, Biochemistry 23 (1984) 4011–4015.
[33] M.F. Brown, R.L. Thurmond, S.W. Dodd, D. Otten, K. Beyer, Elastic deformation of membrane bilayers probed by deuterium NMR relaxation, J. Am. Chem. Soc. 124 (2002) 8471–8484.
[34] K.P. Datema, K.P. Pauls, M. Bloom, Deuterium nuclear magnetic resonance investigation of the exchangeable sites on gramicidin A and gramicidin S in multilamellar vesicles of dipalmitoylphosphatidylcholine, Biochemistry 25 (1986) 3796–3803.
[35] K.C. Lee, S. Huo, T.A. Cross, Lipid peptide interface - valine conformation and dynamics in the gramicidin channel, Biochemistry 34 (1995) 857–867.
[36] W.W. Ying, S.E. Irvine, R.A. Beekman, D.J. Siminovitch, S.O. Smith, Deuterium NMR reveals helix packing interactions in phospholamban, J. Am. Chem. Soc. 122 (2000) 11125–11128.
[37] W. Liu, E. Crocker, D.J. Siminovitch, S.O. Smith, Role of side-chain conformational entropy in transmembrane helix dimerization of glycophorin A, Biophys. J. 84 (2003) 1263–1271.
[38] C. Glaubitz, I.J. Burnett, G. Grobner, A.J. Mason, A. Watts, Deuterium-MAS NMR spectroscopy on oriented membrane proteins: Applications to photointermediates of bacteriorhodopsin, J. Am. Chem. Soc. 121 (1999) 5787–5794.
[39] P.T.F. Williamson, J.A. Watts, G.H. Addona, K.W. Miller, A. Watts, Dynamics and orientation of N+(CD3)(3)-bromoacetylcholine bound to its binding site on the nicotinic acetylcholine receptor, Proc. Natl. Acad. Sci. USA 98 (2001) 2346–2351.
[40] X. Helluy, A. Sebald, Structure and dynamic properties of solid L-tyrosine-ethylester as seen by ^{13}C MAS NMR, J. Phys. Chem. B 107 (2003) 3290–3296.
[41] K. Seidel, M. Etzkorn, L. Sonnenberg, C. Griesinger, A. Sebald, M. Baldus, Studying molecular 3D structure and dynamics by high-resolution solid-state NMR: application to L-tyrosine-ethylester, J. Phys. Chem. 109 (2005) 2436–2442.
[42] N. Giraud, A. Böckmann, A. Lesage, F. Penin, M. Blackledge, L. Emsley, Site-specific backbone dynamics from a crystalline protein by solid-state NMR spectroscopy, J. Am. Chem. Soc. 126 (2004) 11422–11423.
[43] D. Sandström, M. Hong, K. Schmidt-Rohr, Identification and mobility of deuterated residues in peptides and proteins by2H-13C solid-state NMR, Chem. Phys. Lett. 300 (1999) 213–220.
[44] M. Hologne, K. Faelber, A. Diehl, B. Reif, Characterization of dynamics of perdeuterated proteins by MAS solid-state NMR, J. Am. Chem. Soc. 127 (2005).
[45] A.E. McDermott, F.J. Creuzet, A.C. Kolbert, R.G. Griffin, High-resolution magic-angle-spinning NMR spectra of protons in deuterated solids, J. Magn. Reson. 98 (1992) 408–413.
[46] L. Zheng, K.W. Fishbein, R.G. Griffin, J. Herzfeld, Two-dimensional solid-state ^{1}H NMR and proton exchange, J. Am. Chem. Soc. 115 (1993) 6254–6261.
[47] B. Reif, R.G. Griffin, ^{1}H detected ^{1}H,^{15}N correlation spectroscopy in rotating solids, J. Magn. Reson. 160 (2003) 78–83.
[48] V. Chevelkov Rossum, F. Castellani, K. Rehbein, A. Diehl, M. Hohwy, S. Steuernagel, F. Engelke, H. Oschkinat, B. Reif, 1H detection in MAS solid state NMR spectroscopy employing pulsed field gradients for residual solvent suppression, J. Am. Chem. Soc. 125 (2003) 7788–7789.
[49] E.K. Paulson, C.R. Morcombe, V. Gaponenko, B. Dancheck, R.A. Byrd, K.W. Zilm, Sensitive high resolution inverse detection NMR spectroscopy of proteins in the solid state, J. Am. Chem. Soc. 125 (2003) 15831–15836.
[50] B. Reif, C.P. Jaroniec, C.M. Rienstra, M. Hohwy, R.G. Griffin, ^{1}H–^{1}H MAS correlation spectroscopy and distance measurements in a deuterated peptide, J. Magn. Reson. 151 (2001) 320–327.
[51] E.K. Paulson, C.R. Morcombe, V. Gaponenko, B. Dancheck, R.A. Byrd, K.W. Zilm, High-sensitivity observation of dipolar exchange and NOEs between exchangeable protons in proteins by 3D solid-state NMR spectroscopy, J. Am. Chem. Soc. 125 (2003) 14222–14223.
[52] V. Chevelkov, K. Faelber, A. Diehl, U. Heinemann, H. Oschkinat, B. Reif, Detection of dynamic water molecules in a microcrystalline sample of the SH3 domain of alpha-spectrin by MAS solid-state NMR, J. Biomol. NMR 31 (2005) 295–310.
[53] J.L. Markley, I. Putter, O. Jardetzky, High-resolution nuclear magnetic resonance spectra of selectively deuterated staphylococcal nuclease, Science 161 (1968) 1249.

[54] H.R. Kalbitzer, R. Leberman, A. Wittinghofer, H-1-NMR spectroscopy on elongation-factor TU from *Escherichia coli*—resolution enhancement by perdeuteration, FEBS Lett. 180 (1985) 40–42.
[55] D.M. LeMaster, F.M. Richards, NMR sequential assignment of *Escherichia coli* thioredoxin utilizing random fractional deuteration, Biochemistry 27 (1988) 142–150.
[56] D.A. Torchia, S.W. Sparks, A. Bax, Delineation of alpha-helical domains in deuteriated Staphylococcal nuclease by 2D NOE NMR spectroscopy, J. Am. Chem. Soc. 110 (1988) 2320–2321.
[57] D.M. LeMaster, Isotope labeling in solution protein assignment and structural-analysis, Prog. NMR Spectrosc. 26 (1994) 371–419.
[58] O. Millet, D.R. Muhandiram, N.R. Skrynnikov, L.E. Kay, Deuterium spin probes of side-chain dynamics in proteins. 1. Measurement of five relaxation rates per deuteron in C-13-labeled and fractionally H-2-enriched proteins in solution, J. Am. Chem. Soc. 124 (2002) 6439–6448.
[59] N.R. Skrynnikov, O. Millet, L.E. Kay, Deuterium spin probes of side-chain dynamics in proteins. 2. Spectral density mapping and identification of nanosecond time-scale side-chain motions, J. Am. Chem. Soc. 124 (2002) 6449–6460.
[60] A.J. Shaka, P.B. Barker, R. Freeman, Computer-optimized decoupling scheme for wideband applications and low-level operation, J. Magn. Reson. 64 (1985) 547–552.
[61] M. Bak, J.T. Rasmussen, N.C. Nielsen, SIMPSON: a general simulation program for solid-state NMR spectroscopy, J. Magn. Reson. 147 (2000) 296–330.
[62] D. Marks, N. Zumbulyadis, S. Vega, Deuterium cross-polarization magic-angle spinning, J. Magn. Res. A 122 (1996).
[63] C. Auger, A. Lesage, S. Caldarelli, P. Hodgkinson, L. Emsley, Deuterium-carbon NMR correlation spectroscopy in oriented materials, J. Am. Chem. Soc. 119 (1997) 12000.
[64] P. Hodgkinson, C. Auger, L. Emsley, Deuterium to carbon cross-polarization in liquid crystals, J. Chem. Phys. 109 (1998) 1873–1884.
[65] W.H. Press, S.A. Teukolsky, W.T. Vetterling, B.P. Flannery, Numerical recepies in C: the art of scientific computing, Cambridge University Press, Cambridge, 1992.
[66] M.J.D. Powell, A method for minimizing a sum of squares of non-linear functions without calculating derivatives, Comput. J. 7 (1965) 303–307.
[67] A. Schmidt, S. Vega, NMR Line shape analysis for two-site exchange in rotating solids, J. Chem. Phys. 87 (1987) 6895–6907.
[68] M.J. Duer, M.H. Levitt, Time domain calculation of chemical exchange effects in the NMR spectra of rotating solids, Solid State Nucl. Magn. Reson. 1 (1992) 211–215.
[69] R.H. Merson, in: Proceedings of a Symposium on Data Processing, South Australia, 1947.
[70] T.H. Huang, R.P. Skarjune, R.J. Wittebort, R.G. Griffin, E. Oldfield, Restricted rotational isomerization in polymethylene chains, J. Am. Chem. Soc. 102 (1980) 7377–7379.
[71] A. Abragam, Principles of Nuclear Magnetism, International Series of Monographs on Physics, Clarendon Press, Oxford, 1961.
[72] A.D. Ronemus, R.R. Vold, R.L. Vold, Deuterium quadrupole-echo studies of molecular motion in a biphenyl-P-cyclodextrin clathrate, J. Chem. Soc., Faraday Trans. 84 (1988) 3761–3776.
[73] K. Beshah, R.G. Griffin, Deuterium quadrupole echo NMR study of methyl group dynamics in *N*-acetyl-DL-(γ-d6)-valine, J. Magn. Res. 84 (1989) 268–274.
[74] M.H. Levitt, Composite pulses, Prog. NMR Spectrosc. 18 (1986) 61–122.
[75] H.W. Spiess, NMR Basic Principles and Progress Rotation of Molecules and Nuclear Spin Relaxation, Springer, Berlin, 1978.
[76] D.A. Torchia, A. Szabo, Spin–lattice relaxation in solids, J. Magn. Reson. 49 (1982) 107–121.
[77] M. Mehring, Principles of High Resolution NMR in Solids, Springer, Berlin, 1983.